J IRAN CHEM SOC (2017) 14:541–549
DOI 10.1007/s13738-016-1002-z

ORIGINAL PAPER

A novel dual thermo- and pH-responsive silver nanocomposite hydrogel as a drug delivery system

Zari Hooshyar[1] · **Ghasem Rezanejade Bardajee**[1]

Received: 15 May 2016 / Accepted: 31 October 2016 / Published online: 23 November 2016

Abstract The purpose of this study was to develop a novel dual thermo- and pH-responsive silver nanocomposite hydrogel (SNH) for drug release applications. This smart SNH was prepared in a facile one-pot method by in situ reduction of silver ions in salep solution and then grafting of poly(vinylpyrrolidone-co-acrylic acid) onto it. The SNH was characterized by transmission electron microscopy (TEM), scanning electron microscopy with energy-dispersive X-ray analysis (SEM–EDAX), thermo-gravimetric analysis (TGA), Fourier transform infrared (FT-IR), UV–Vis spectroscopy, and cyclic voltammetry. The dependence of swelling properties of the prepared SNH on the reaction variables (such as monomer, Ag NO_3, and cross-linker concentrations), temperature, pH, and salt was investigated. The potential of obtained SNH was examined for the deferasirox release from prepared hydrogel under different temperatures and pHs. The evaluation of release mechanism and determination of diffusion coefficients were also studied. In addition, SNH showed good antibacterial potentials. The results of this study provide valuable information regarding the development of dual stimuli-sensitive SNH for biomedical applications.

Keywords Ag nanoparticle · Nanocomposite hydrogels · Drug delivery · Swelling

✉ Ghasem Rezanejade Bardajee
rezanejad@pnu.ac.ir

[1] Department of Chemistry, Payame Noor University, PO BOX 19395-3697, Tehran, Iran

Introduction

Drug delivery refers to method or process of administering a pharmaceutical compound in the body as needed to achieve its desired therapeutic effect [1, 2]. During recent decades, the drug delivery vehicle is transformed into nanocomposite hydrogels because they frequently exhibit remarkably improved properties compared with the pure hydrogels [3, 4]. Hydrogels are three-dimensional cross-linked hydrophilic polymers that are able to absorb and retain a large quantity of water, saline, and physiological solutions [5, 6]. Because of their significant water uptake capacity and flexibility, hydrogels mimic biological tissues and have extensive applications in medical application and tissue engineering [7]. Most hydrogels show an active and significant response to small changes in the surrounding environment such as temperature, pH, ionic strength, electric field, and light [8]. The temperature and pH are two important factors in biological systems [9]. Because of the temperature in human body is usually higher than room temperature, temperature-responsive hydrogels have been fabricated by poly(isopropylacrylamide), poly(vinylpyrrolidone) (PVP), and poly(ethylene glycol)-polyester block copolymers to use in oral drug delivery [8, 10–13]. As we know for drug transportation from stomach to intestine in oral administration, pH-sensitive hydrogels have been prepared by poly(acrylic acid) (PAA) and its derivatives. Therefore, drug release behavior of dual thermo- and pH-responsive hydrogels can be triggered by changing the chemical structure of the pH- and temperature-sensitive polymers, leading to enhanced specificity of drug delivery and less side effects [14, 15].

It is well known that nanoparticles embedded in hydrogels increase the stability of drug and provide a slower and more continuous release mode of drugs [16–19]. It

is reported that noble metal nanoparticles such as silver, gold, and platinum have been normally used in biological pathways to achieve drug delivery to cellular and intracellular targets [17, 18]. Among them, silver nanoparticles (Ag NPs) have been extensively studied and used in medical devices and pharmaceutical products because of their unique chemical and physical properties and pronounced antibacterial activity [17–19]. Silver nanocomposite hydrogels (SNH) can be synthesized by preparation of Ag NPs and hydrogels separately and then physically combining them, or by mixing pre-made Ag NPs with a hydrogel precursor followed by gelation [20–23]. However, these methods involved toxic chemical as a stabilizing reagent and complicated physical techniques such as sputtering and plasma deposition. Recently, we have shown a facile one-pot and cheap method for preparation of the pH-sensitive SNH [24]. It was demonstrated that Ag NPs can be successfully synthesized in salep solutions (as a reducing agent) via sunlight UV-irradiation [25]. In the presence of a capping agent, sunlight-UV as UV-irradiation can promote the reduction of the Ag^+ into nano-Ag [24, 25]. Salep is glucomannan-based powdery substance extracted from dried tubers of certain natural terrestrial orchids [26]. It is a non-toxic biocompatible, biodegradable, and water-soluble polysaccharide to normalize blood sugar and relieve stress on the pancreas and discourage blood [27]. It has unique potentials for use in various fields because of its nutritive and demulcent properties [28]. In situ reduction of Ag^+ was done by simultaneously anchoring of salep functional groups (hydroxyl groups of glucomannan repeating units) to Ag ions and reduction process via sunlight UV-irradiation [24, 25]. To give pH-sensitive SNH, the reaction was followed by graft copolymerization of AA onto salep-(nano-Ag) composite [24].

The aim of this work was to develop a novel dual thermo- and pH-responsive SNH from P (VP-co-AA) grafted onto salep for deferasirox release applications. Some additional results concerning the influence of VP/AA ratio, cross-linker, and $AgNO_3$ concentrations on the swelling properties of synthesized SNH were investigated. Furthermore, the temperature and pH responsively of the obtained SNH were determined by swelling data. Structural and morphological characterizations of this smart SNH were carried out by transmission electron microscopy (TEM), scanning electron microscopy with energy-dispersive X-ray analysis (SEM–EDAX), thermo-gravimetric analysis (TGA), Fourier transform infrared (FT-IR), UV–Vis spectroscopy, and cyclic voltammetry. In addition, antibacterial potential of investigated SNH was tested. The results indicate that our dual thermo- and pH-responsive SNH have been the best candidate for different biomedical applications.

Experimental

Chemicals

Salep was supplied from Kordestan, Iran ($M_n = 1.17 \times 10^6$ g/mol, $M_w = 1.64 \times 10^6$ g/mol, PDI = 1.39, eluent = water, flow rate =1 mL/min, and acquisition interval = 0.43 s from GPC results). Acrylic acid (AA, 98%), vinylpyrrolidone (VP), and methylenebisacrylamide (MBA, 99%) were obtained from Merck. Silver nitrate ($AgNO_3$, 99%), sodium, chloride (NaCl, 99%), calcium chloride ($CaCl_2$, 99%), urea, and ammonium persulfate (APS, 99%) were purchased from Fluka. Deferasirox was obtained from Osveh Pharmaceutical Co., Tehran, Iran, as a gift. Gram-negative *Escherichia coli* (*E. coli*) and Gram-positive *Staphylococcus aureus* (*S. aureus*) bacteria were prepared from NIGEB Bacterial Bank (Tehran, Iran). All other chemicals were of laboratory grade and were used as received. The water added in all experiments was double-distilled water.

Equipment

Absorption spectra were measured on a Shimadzu UV–visible 1650 PC spectrophotometer. FT-IR spectra were recorded using a Jasco 4200 FT-IR spectrophotometer. Scanning electron microscopy (SEM) images and energy-dispersive X-ray analysis (EDAX) were obtained with Hitachi S-5200 SEMEDAX operated at 10 kV after coating the dried samples with gold films. Transmission electron microscopy (TEM) images were captured using a Zeiss TEM at an acceleration voltage of 80 kV. Thermo-gravimetric analysis (TGA) were carried out on a TA instrument 2050 thermo-gravimetric (TG) analyzer under N_2 atmosphere (25 mL/min) at a scan rate of 20 °C/min. Voltammetric measurements were taken with a computer-controlled electrochemical system using a AUTULAB PGSTAT12 with glassy carbon (GC) electrode as a working electrode, platinum wire as a auxiliary electrode, and AgCl/Ag as a reference electrode.

Synthesis of SNH

Scheme 1 depicts a possible mechanism for the preparation of SNH. At first, 1 g of salep was dissolved in 80 mL of double-distilled water with continuous mechanical stirring (200 rpm) until a homogeneous viscous mixture was obtained, and then, 5 mL of the $AgNO_3$ solution (0, 2, 6, 12, and 18 mg/mL) was added dropwise with continuous stirring. After 30 min, the reactor was transferred into thermostated water bath preset at desired temperature (80 °C). Then, 5 mL of AA /VP solution (0.5, 1, 1.5, and 2 mg/mL),

Scheme 1 Proposed mechanism for preparation of SNH

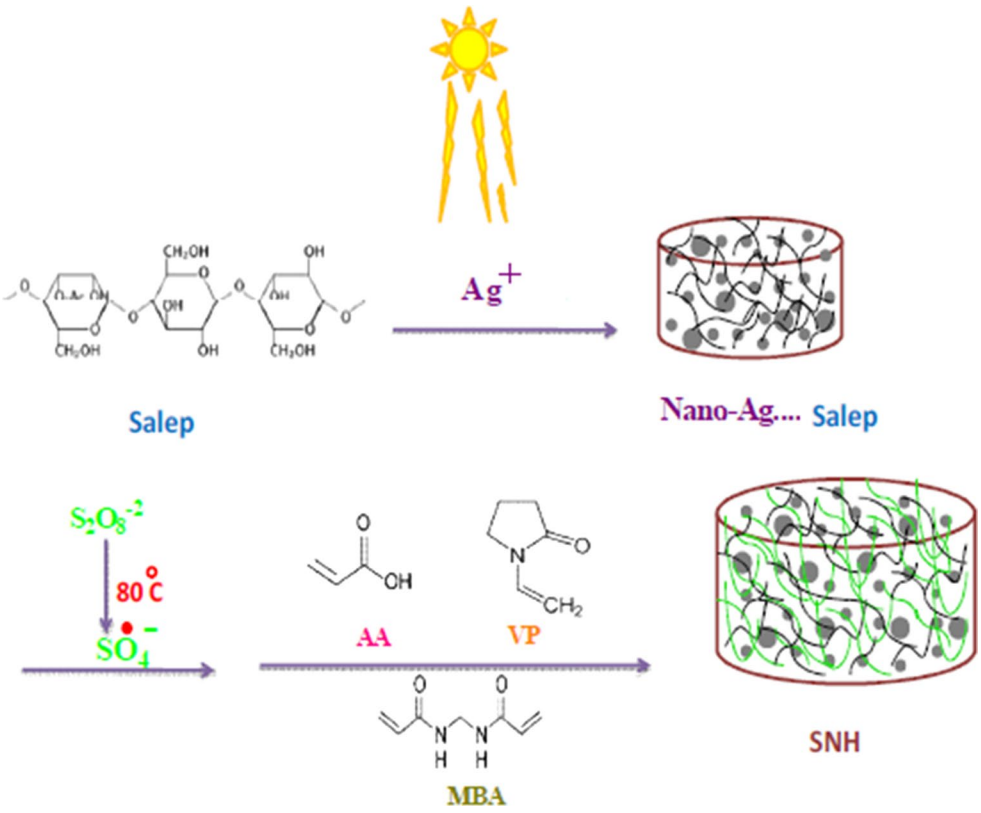

5 mL of the MBA (6, 10, 14, and 18 mg/mL), and 5 mL of APS (6, 10, 14, and 18 mg/mL) were added and the reaction mixture was stirred for 30 min. The reaction mixture was poured into 100 mL of ethanol and dried under vacuum at 40 °C to constant weight and subjected to the extraction with the water as solvent to remove uncrosslinked polymer and/or residual monomer. Extracted hydrogel composite was dried again in a vacuum to the constant weight and stored in the absence of moisture, heat, and light to further characterization.

Swelling studies

Swelling properties of SNH were investigated by gravimetric method. In this way, a tea bag (i.e., a 100.00-mesh nylon screen) containing 0.50 g of SNH was immersed in swelling medium, and at predetermined time intervals, the weights of swollen hydrogels were measured. Swelling degree was determined from the following equation [24]:

$$\text{Swelling degree (g/g)} = (\text{Weight of swollen gel/Weight of dried gel}) - 1$$

Absorbency under load (AUL)

In a Petri dish ($d = 118$ mm and $h = 12$ mm) containing double-distilled water, a macro-porous sintered glass filter plate (porosity# 0, $d = 80$ mm, and $h = 7$ mm) with a polyester gauze was placed and a 0.5 g SNH was uniformly placed on the surface of a polyester gauze. To reach the desired load (applied pressure 0.3 and 0.9 psi) onto SNH, a cylindrical solid weight (Teflon, $d = 60$ mm of variable height) which could slip freely in a glass cylinder ($d = 60$ mm and $h = 50$ mm) was used. Note that the liquid level was equal to the height of the sintered glass filter. After predetermined time intervals, the swollen SNH was weighed to calculate the AUL value according to above equation.

Drug release from SNH

5 mL of deferasirox solution (0.038 mg/mL) was mixed with SNH (0.05 g) and allowed the SNH to completely swell in the drug solution. After that, it was dried and dispersed in 20 mL phosphate buffer (pH = 2 and 7) in a rotary shaker (200 rpm) at 25 and 37 °C. At various time points, 1 mL filtered sample was taken out for determination of the release process. The concentration of deferasirox release was quantitatively analyzed by UV–visible spectroscopy at wavelength of 297 nm.

Antimicrobial testing

Disk diffusion method was used to study the antibacterial activity of SNH. At first, Gram-positive *S. aureus* and

Gram-negative *E. coli* bacteria were cultivated at 37 °C on the surface of LB nutrient agar plates, and then, SNH, ampicillin, and $AgNO_3$ were placed on them. The plates were incubated at 37 °C for 24 h. The antibacterial effect of samples was recorded by inhibition zone appeared around the samples.

Results and discussions

Swelling

The concentration of salep plays an important role in the formation and swelling properties of hydrogels. Our previous study showed that in order to prepare continuous hydrogels from salep, its concentration would be well 1 mg/mL [27, 28]. In lower salep concentrations, the hydrogels disintegrate in water immediately after immersion, while in higher salep concentrations, stiffer hydrogels are obtained and they need longer times for reaching swelling equilibrium which make them improper for drug delivery application [29]. Therefore, in this work, we investigated the effect of molar ratio of AA/VP, $AgNO_3$, MBA, and APS concentrations on the water swelling degree of SNH in double-distilled water at 25 °C (Fig. 1). It was clear that the water swelling capacity of the prepared SNH was sensitive to all these variables.

Figure 1a shows the swelling of SNH with various contents of $AgNO_3$. It is obvious that the swelling degree of SNH gradually decrease with the increase in $AgNO_3$ loading. This phenomenon is ascribed to the restriction of segmental motion of the polymer chains and partial occupation of free space by Ag NPs. Moreover, Ag NPs can form new network with some hydroxyl and carboxylate groups of the hydrogel networks and prevent the water penetration and diminish the water swelling capacity [24].

Swelling behavior of SNH in Fig. 1b reveals that the swelling degree of the SNH is highly dependent on the content of the MBA. The swelling degree decreased with increasing the content of the MBA. This swelling behavior of the SNH may be attributed to the increase in cross-linking density derived from the increased MBA. In fact, more three-dimensional polymer networks were formed in high cross-linker content, which could prevent the water penetration into the SNH structure [28].

The obtained results also show that the swelling of SNH strongly depends on the concentration of APS (Fig. 1c). Increasing the APS content to 10 mg/mL caused an immense increase in swelling degree due to a quick polymerization of AA and VP, which resulted in the formation of more hydrophilic groups grafted on the chain of the composite, and the inside osmotic pressure of the reticular structure was enhanced. However, when the APS concentration was higher than about 10 mg/mL, the branched chains of small molecules turn longer and consequently block the mesh structure and restrict the expansion of SNH [29].

With the increase in molar ratio of AA/VP (Fig. 1d), the swelling degree of SNH first increased due to the increased grafting rate and the grafted chain. When the value of molar ratio of AA/VP was higher than 1, the swelling capacity of SNH reduced due to the predominant homopolymerization phenomenon in the reaction system and weakened the grafting rate [29]. In the remainder of this manuscript, the SNH sample with $C_{AgNO3} = 2$ mg/mL, $C_{MBA} = 6$ mg/mL, $C_{APS} = 10$ mg/mL, and molar ratio of AA/VP= 1 was used for further investigations due to its highest swelling degree.

Figure 2a shows swelling kinetics of SNH in double-distilled water at 25, 37, 50, and 60 °C. It is noticed that swelling degree reached nearly plateau at around 240 min after immersing the formed SNH in water for all temperature. It can be seen that with the increase in temperature, the water swelling degree of the SNH decreased. The reason could be illustrated to an intramolecular hydrogen bond. At low temperature and initial immersing time, water penetrating into the hydrogel was in a bound state. When temperature was raised from 25 to 60 °C, the interactions between hydrophobic groups overcome on the hydrogen bonds. Therefore, a part of hydrogen bonds that existed in the network structure were destroyed and cause to the phase separation. Consequently, the SNH would become less hydrophilic and had lower swelling capacity [27].

The important parameters affecting the swelling process is pH value of solution. In order to investigate the influence of pH values on water swelling capacity, the swelling behavior of the prepared SNH was studied in the pH range of 2–10. Figure 2b shows that the swelling behavior of prepared SNH was depended on pH, which reflected the pH stimuli-responsive properties. As it can be seen, the swelling of the SNH increased slowly with increasing the pH from 2 to 8 and then decreased. This pH-dependent swelling behavior is due to the carboxylate groups of AA monomer. At acidic pHs, carboxylic acid groups are protonated and form hydrogen bonds in the networks and render the networks more hydrophobic. In contrast, at basic pHs, carboxylic acid groups are un-protonated and the electrostatic repulsion between these charged groups increases. By increasing the electrostatic repulsion, osmotic pressure increases, and thus, hydration of the SNH enhances. In higher basic solutions (8 < pH), the rising concentration of OH^- outside the SNH in water can give rise to an osmotic pressure that causes the hydrogel to shrink (higher ionic strength) [26]. Dual stimuli-sensitive SNH was also investigated. The SNH showed an increase in swelling in response to both stimuli (pH and temperature, see insert of Fig. 2b).

In order to investigate the response behaviors of the SNH in biological environment, we prepared salt solutions

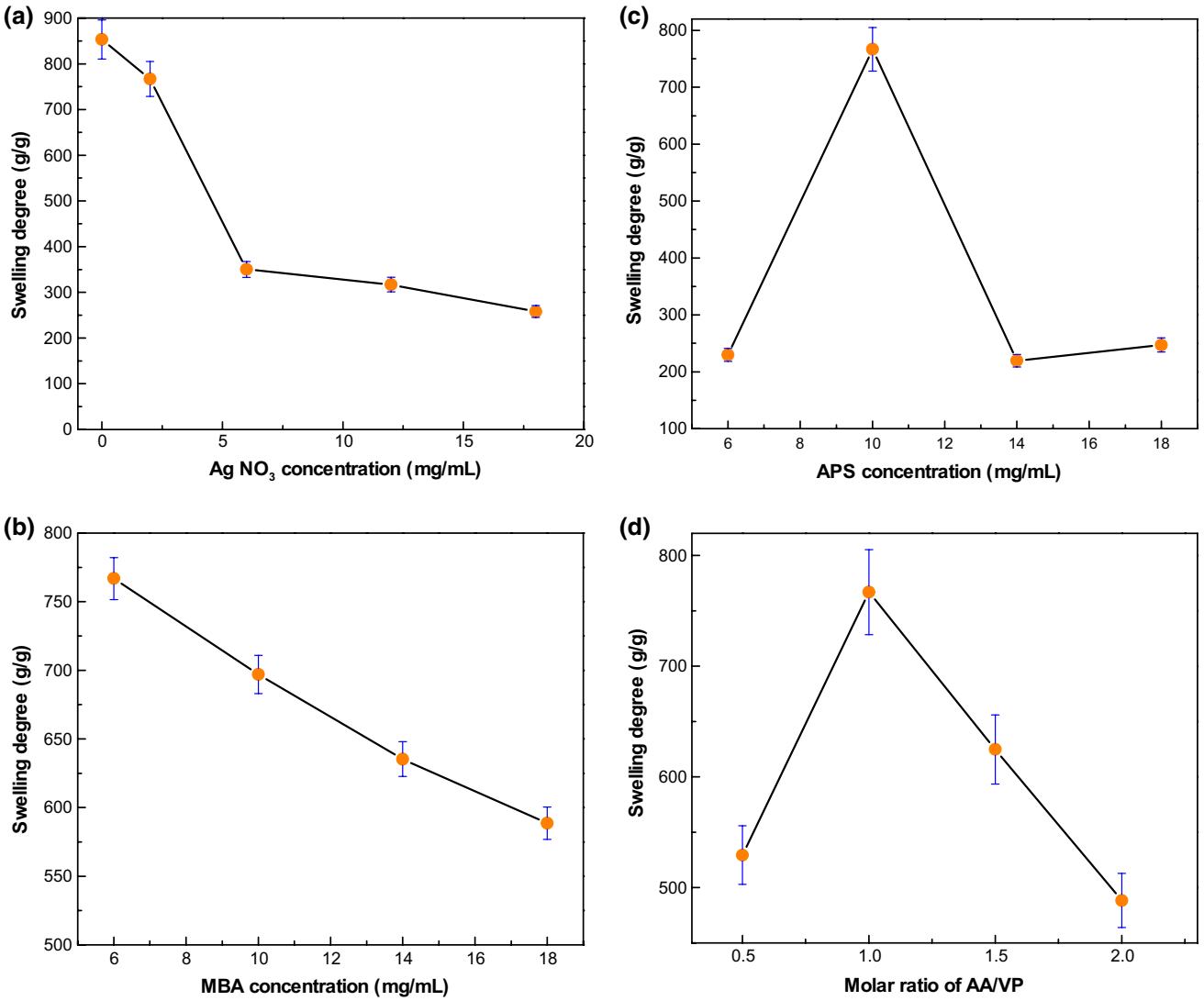

Fig. 1 The effect of **a** $AgNO_3$ concentrations (C_{MBA} = 6 mg/mL, C_{APS} = 10 mg/mL, and molar ratio of AA/VP = 1), **b** MBA concentrations (C_{AgNO3} = 2 mg/mL, C_{APS} = 10 mg/mL, and molar ratio of AA/VP = 1), **c** APS concentrations (C_{AgNO3} = 2 mg/mL, C_{MBA} = 6 mg/mL, and molar ratio of AA/VP = 1), and **d** molar ratio of AA/VP (C_{AgNO3} = 2 mg/mL, C_{MBA} = 6 mg/mL, and C_{APS} = 10 mg/mL) on the water swelling degree of SNH in double-distilled water at 25 °C

of urea, $CaCl_2$, and NaCl (the double-distilled water as a control group) with 0.9wt% concentration (equivalent of the concentration of physiological saline). As shown in Fig. 2c, the swelling ratio of SNH appears a certain decreasing trend in the order of urea, $CaCl_2$, and NaCl solutions compared to that of the double-distilled water. In $CaCl_2$ and NaCl solutions, the swelling ratio decreased due to the charge shielding of Ca^{2+} and Na^+ will impair electrostatic repulsion of anion in the polymer chain. However, in urea solution, the decrease in electrostatic repulsion is not significant and the partial ionization of the carboxyl groups and the formation of COO^- groups are conductive to improve the swelling ratio [30].

AUL is a great important parameter in various industrial applications such as irrigation systems in agriculture which is often given in the technical data sheets and patent articles [29, 30]. Also, AUL can be reflected on as evaluate of the gel strength of the hydrogel and many attempts have been made to reach hydrogel with high AUL or high strengths of the swollen gel [29]. Thus, we studied AUL effect by using a simple AUL tester at 0.3 and 0.9 psi. As shown in Fig. 2d, the swelling ratio slowly increased and then begins to level off. In addition, the AUL decreased by increasing the amount of loading. The results show that our synthesized SNH was very resistant against applied pressure increase [31].

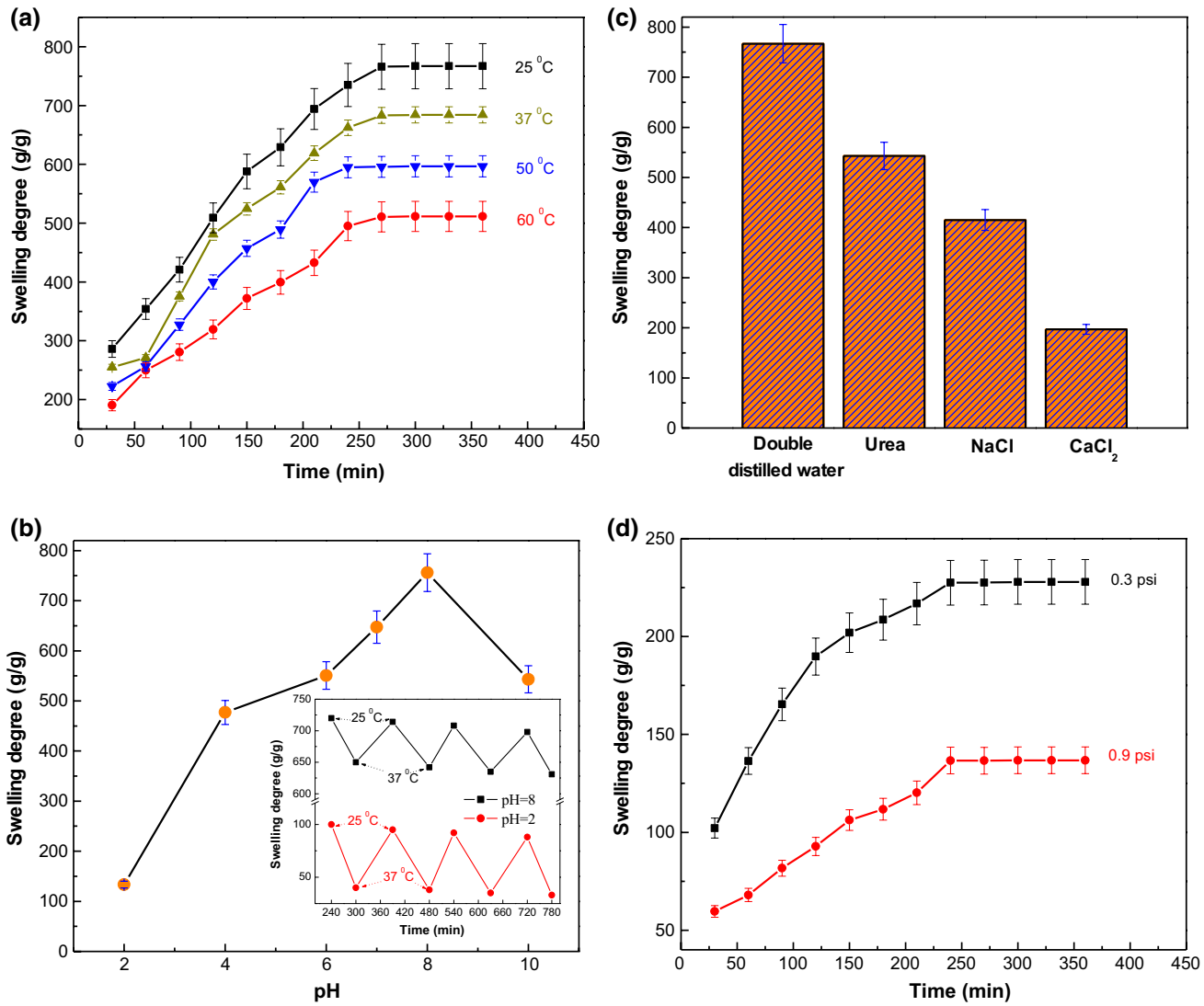

Fig. 2 The effect of **a** temperature, **b** pH, **c** salt, and **d** AUL on the swelling ratio of SNH. *Inset* of Fig. 2b shows the on–off switching behavior (at phosphate buffer (pH = 2 and 7) at 25 and 37 °C) of the SNH

Characterization

FT-IR spectra of the initial substrates and result materials are shown in Fig. 3a. FT-IR spectra of salep exhibit a large number of hydroxyl and carboxylic groups evidence by the strong O–H (3500–3200 cm^{-1}) and C=O (1580 cm^{-1}) peaks. FT-IR spectra of PAA show the stretching vibration of the carboxylic groups (1728 cm^{-1}) and O–H stretching (3300 cm^{-1}). FT-IR spectra of PVP show the stretching vibration of C–H from alkyl groups (3000–2800 cm^{-1}) and the stretching vibration of C=O and C–O (1750–1690 cm^{-1}). FT-IR spectra of P(AA-co-VP)-g-salep reveal that all of the characteristic peaks of salep, PAA, and PVP, while formation of Ag NPs in P(AA-co-VP)-g-salep, slightly shift the stretching vibrations peaks of P(AA-co-VP)-g-salep. These peak shift could be due to the formation of coordination bond between the nano-Ag and the electron-rich groups (such as C=O and OH) present in the hydrogel network.

To confirm the formation of Ag NPs in hydrogel, UV–visible spectroscopy was used. It was previously proved that a characteristic absorption band at around 410 nm attributed to the surface Plasmon resonance (SPR) effect of Ag NP [32]. The absorption spectra of the P(AA-co-VP)-g-salep and SNH are shown in Fig. 3b. As observed, there is one band at around 410 nm in SNH, while there is no such band in the P(AA-co-VP)-g-salep.

To indicate the presence of Ag NP in hydrogel, cyclic voltammogram of SNH was recorded with 100 mV/s voltage scan rate from −1.5 to 0.1 V. Prior to each run, the

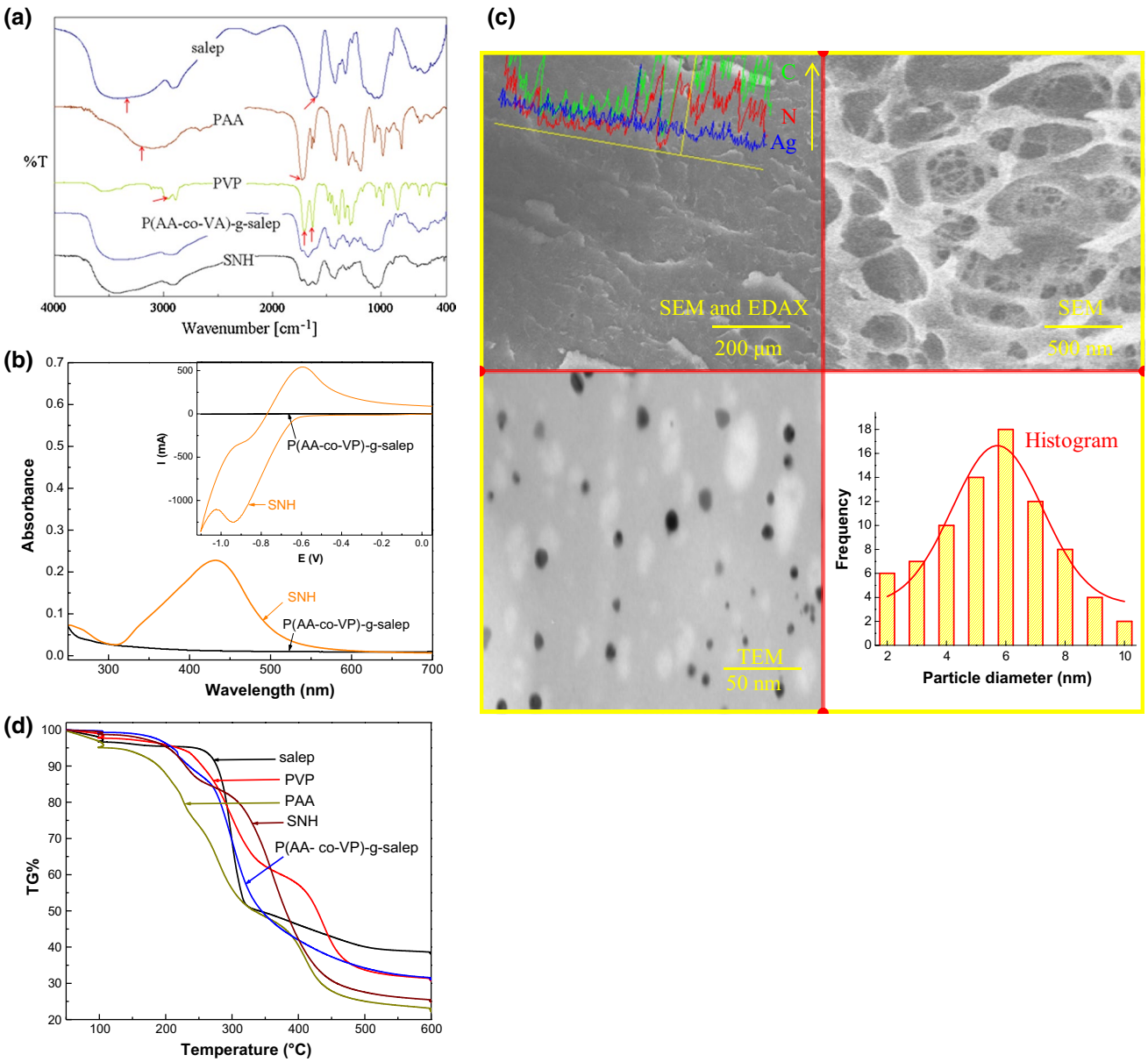

Fig. 3 **a** FT-IR spectra of salep, PAA, PVP, P(AA-co-VP)-g-salep, and SNH, **b** absorption spectra (*Inset*: cyclic voltammogram) of SNH, **c** SEM, EDAX, TEM, and related histogram, and **d** TGA of salep, PAA, PVP, P(AA-co-VP)-g-salep, and SNH

GC electrode was polished with 0.1 mm alumina powder and washed with distilled water. Insert of Fig. 3b shows a couple of quasi-reversible cyclic voltammogram profiles of SNH with well-defined redox peak at −0.93 mV and the oxidation peak at −0.61 V. Moreover, a cyclic voltammogram of P(AA-co-VP)-g-salep was run in affirmation condition, which showed no electroactivity in the potential range of our interest (−1.5 to 0.1 V). These results confirmed the electrochemical behaviors of the SNH.

Morphology of the surface and cross section of the SNH are presented in Fig. 3c. The SEM reveals that the SNH surface is smooth. The cross-sectional images exhibit the well-defined interconnected 3D porous network of the produced SNH. The pores sizes of SNH are in the range of sub-micrometer to several micrometers, and the walls of these pores are composed by randomly cross-linked monomers. EDAX spectra are inserted in SEM image. As can be seen, there are three color peaks in EDAX spectra which are related to C (green peak), N (red peak), and Ag (blue peak). Each peak shows the sensitivity of EDAX instrument to that element in the defined reign (yellow line). Therefore, the results of EDAX spectra confirm the presence of C, N, and Ag element in the SNH sample. TEM images of the SNH proved that the NPs are uniformly distributed on

the surface of the SNH without severe aggregation and the microspheres had good distribution of element silver with nanometric size (<10 nm).

Furthermore, the thermal stability of SNH was compared with the thermal stability of salep, PAA, PVP, and P(AA-co-VP)-g-salep. Results of the variation of mass with temperature are shown in Fig. 3d. Due to the different structures for the entitled samples, the TGA curves of the aforementioned samples were completely different from each other. TGA curve of pure salep shows the first mass loss stages (35–160 °C) corresponded to loss of the water in the polymer (characteristic of its hydrophilicity) and the second mass loss (250–310 °C) due to degradation of the polymer chains. The thermal degradations of PAA and PVP involve multiple steps assigned to the presence of weak head-to-head linkages, scission of unsaturated terminal groups, and random scission of the carbon–carbon main chain. Degradations start at almost 175 °C and 235 for PAA and PVP, respectively, while degradation starts near 207 °C for the P(AA-co-VP)-g-salep. The different starting degradation temperature for P(AA-co-VP)-g-salep is attributed to the existence of PVP and PAA into salep biopolymer. The distinct peaks were observed in P(AA-co-VP)-g-salep and SNH. These peaks are attributed to the degradation of weak links inside the macromolecular chain and random chain scission. Therefore, incorporation of the Ag NPs shifts the main degradation steps of P(AA-co-VP)-g-salep resulting in protection of the material from thermal degradation.

Drug release

The effects of pH and temperature on the kinetics of deferasirox release from the SNH were studied. The release profile of deferasirox from SNH is shown in Fig. 4. At pH 2, the less amount of deferasirox is released from SNH as compared to the release of deferasirox at pH 8. This phenomenon is attributed to the swelling pattern of the SNH, where the higher swelling is observed at pH 8. In addition, the release rate at 37 °C is higher than release rate at 25 °C. This behavior at temperature (37 °C) above is attributed to collapse the three-dimensional polymeric network of SNH. Therefore, SNH cannot close the pore tightly and allow releasing the entrapped deferasirox [33, 34].

In order to characterize the release mechanism, Korsmeyer kinetic model (with the help of Eq. 1[36]) is used to calculate the kinetic parameters of deferasirox release from SNH.

$$\mathrm{Log}(M_t/M_\infty) = \log k + n \log t \quad (1)$$

where, M_t and M_∞ are the masses (g) of drug released at time t and equilibrium state, respectively; k is the release rate constant which considers structural and geometric

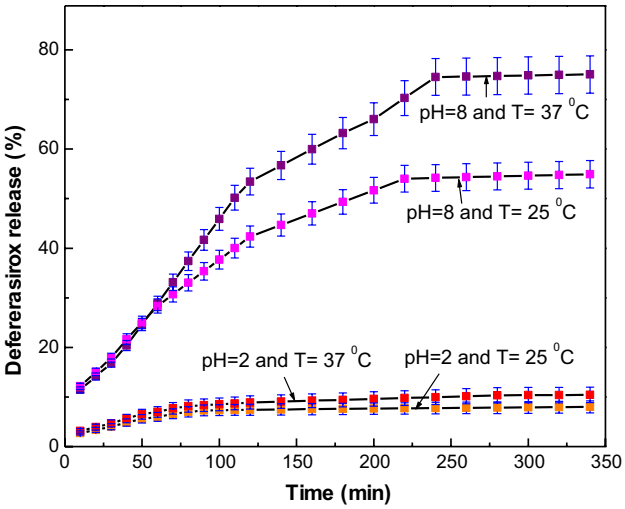

Fig. 4 Release profile of deferasirox from SNH at different temperatures and pHs

characteristics of the release system; and n is the diffusion exponent or release exponent which is indicative of the mechanism of drug release. The n and k values are determined from the slope and intercept of the plot of log (M_t/M_∞) against log t, respectively (Table 1). It can be seen that the diffusion exponents for the SNH in different conditions were less than 0.45. According to the literatures, $n < 0.45$ correspond to a purely Fickian diffusion mechanism, $n > 0.89$ indicate a relaxation-controlled mechanism, and $0.45 < n < 0.89$ indicate an anomalous diffusion mechanism [32–35]. Therefore, the drug release mechanism from SNH is purely Fickian diffusion mechanism.

Antibacterial assay

The antibacterial activity of the SNH was evaluated by disk diffusion method. Figure 5 compares the antibacterial effectiveness of SNH with ampicillin and $AgNO_3$ on *E. coli* and *S. aureus*. As one can see, the antibacterial activities of SNH and $AgNO_3$ on *S. aureus* are similar and both of them are less when compared with ampicillin. However, the number of colonies grown surrounding the SNH found

Table 1 Release exponent (n), rate constant (log k), and correlation coefficient (R^2) for deferasirox release from SNH at different conditions

Condition	log k	n	R^2
pH = 2 and T = 25 °C	1.01	0.35	0.99
pH = 2 and T=37 °C	1.05	0.39	0.99
pH = 8 and T=25 °C	1.04	0.37	0.98
pH = 8 and T=37 °C	1.03	0.38	0.98

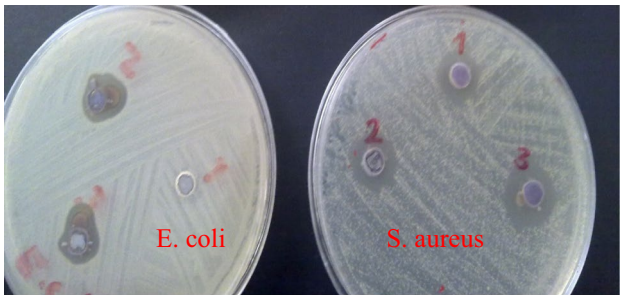

Fig. 5 Antibacterial test results for *E. coli* and *S. aureus* after 24 h incubation. 1–3 are SNH, $AgNO_3$, and ampicillin, respectively

to be almost nil on *E. coli*. Further study on the antibacterial activity of SNH is under survey, and we will report the results in the near future.

Conclusion

Taken together, the results of this study demonstrate dual thermo- and pH-responsive SNH. This smart SNH was synthesized by in situ reduction of silver ions in salep solution and then grafting of P(VP-co-AA) onto it. FT-IR and TGA studies showed chemical interaction between Ag NPs and P(VP-co-AA)-g-salep. The SEM showed that the prepared SNH had porous in nature. The TEM and EDAX image proved the presence of Ag NPs with size <10 nm in P(VP-co-AA)-g-salep. Besides, the SNH showed considerable temperature and pH sensitivity for the in vitro release of deferasirox. The in vitro antibacterial activities test showed antibacterial activities of the SNH against *S. aureus*. Therefore, the SNH has potential as a new approach for biomedical applications.

Acknowledgements The authors wish to thank Payame Noor University for its financial support of this study.

References

1. K. Krukiewicz, J.K. Zak, Mater. Sci. Eng. C **62**, 927 (2016)
2. H. Hamidian, T. Tavakoli, Carbohydr. Polym. **144**, 140 (2016)
3. D. Pathania, D. Gupta, N.C. Kothiyal, Int. J. Biol. Macromol. **84**, 340 (2016)
4. M. Yadollahi, S. Farhoudian, S. Barkhordari, I. Gholamali, H. Farhadnejad, H. Motasadizadeh, Int. J. Biol. Macromol. **82**, 273 (2016)
5. M. Saboktakin, R.M. Tabatabaei, Int. J. Biol. Macromol. **75**, 426 (2015)
6. M. Zhong, F. Shi, Y. Liu, X. Liu, X. Xie, Chin. Chem. Lett. **27**, 312 (2016)
7. M. Yadollahi, S. Farhoudian, H. Namazi, Int. J. Biol. Macromol. **79**, 37 (2015)
8. A. Hebeish, S. Farag, S. Sharaf, T. Shaheen, Int. J. Biol. Macromol. **81**, 356 (2015)
9. M. Xia, W. Wu, F. Liu, P. Theato, M. Zhu, Eur. Polym. J. **69**, 472 (2015)
10. J. Spasojević, A. Radosavljević, J. Krstić, D. Jovanović, V. Spasojević, M. Kalagasidis-Krušić, Z. Kačarević-Popović, Eur. Polym. J. **69**, 168 (2015)
11. K. Akamatsu, M. Shimada, T. Tsuruoka, H. Nawafune, S. Fujii, Y. Nakamura, Langmuir **26**, 1254 (2010)
12. Y. Moon, G. Jung, J. Yun, H. Kim, Mater. Sci. Eng. B **2013**, 178 (1097)
13. P. Schexnailder, G. Schmidt, Colloid Polym. Sci. **287**, 1 (2009)
14. M. Casolaro, I. Casolaro, J. Drug Deliv. Sci. Technol. **30**, 82 (2015)
15. G.R. Mahdavinia, H. Etemadi, Mater. Sci. Eng. C **45**, 250 (2014)
16. S. Bhowmick, V. Koul, Mater. Sci. Eng. C **59**, 109 (2016)
17. E. Kayalvizhy, P. Pazhanisamy, Int. J. Biol. Macromol. **86**, 721 (2016)
18. S. Ravindra, A.F. Mulaba-Bafubiandi, V. Rajinikanth, K. Varaprasad, N.N. Reddy, K.M. Raju, J. Inorg. Organomet. Polym. Mater. **22**, 1254 (2012)
19. M. Bikram, A.M. Gobin, R.E. Whitmire, J.L. West, J. Control. Release **123**, 219 (2007)
20. A.R. Silva, G. Unali, Nanotechnology **22**, 315605 (2011)
21. M.B. Ahmad, M.Y. Tay, K. Shameli, M.Z. Hussein, J.J. Lim, Int. J. Mol. Sci. **12**, 4872 (2011)
22. M. Yadollahi, H. Namazi, M. Aghazadeh, Int. J. Biol. Macromol. **79**, 269 (2015)
23. J. Stojkovska, D. Kostić, Ž. Jovanović, M. Vukašinović-Sekulić, V. Mišković-Stanković, B. Obradović, Carbohydr. Polym. **111**, 305 (2014)
24. G.R. Bardajee, Z. Hooshyar, H. Rezanezhad, J. Inorg. Biochem. **117**, 367 (2012)
25. A. Pourjavadi, R. Soleyman, Mater. Res. Bull. **2011**, 46 (1860)
26. G.R. Bardajee, Z. Hooshyar, Carbohydr. Polym. **101**, 741 (2014)
27. G.R. Bardajee, Z. Hooshyar, M. Jahanbakhsh Asli, F.E. Shahidi, N. Dianatnejad, Mater. Sci. Eng. C **36**, 277 (2014)
28. G.R. Bardajee, A. Pourjavadi, R. Soleyman, N. Sheikh, Nucl. Instrum. Methods B **266**, 3932 (2008)
29. G.R. Bardajee, A. Pourjavadi, R. Soleyman, Colloids Surf. A **392**, 16 (2011)
30. S. Dutta, D. Dhara, Polymer **76**, 62 (2015)
31. A. Pourjavadi, P. Eftekhar Jahromi, F. Seidi, H. Salimi, Carbohydr. Polym. **79**, 933 (2010)
32. M. Rehan, H.M. Mashaly, S. Mowafi, A. Abou El-Kheir, H.E. Emam, Dyes Pigments **118**, 9 (2015)
33. A. Cojocariu, L. Profire, M. Aflori, C. Vasile, Appl. Clay Sci. **57**, 1 (2012)
34. A. Giri, T. Ghosh, A.B. Panda, S. Pal, A. Bandyopdhyay, Carbohydr. Polym. **87**, 1532 (2012)
35. G.R. Bardajee, Z. Hooshyar, J. Polym. Res. **20**, 298 (2013)